ELSEVIER

Journal of Atmospheric and Solar-Terrestrial Physics 69 (2007) 322–333

Journal of ATMOSPHERIC AND SOLAR-TERRESTRIAL PHYSICS

www.elsevier.com/locate/jastp

Multiple plasmapause undulations observed by the IMAGE satellite on 20 March 2001

J. Goldstein[a,*], B.R. Sandel[b], H.U. Frey[c], S.B. Mende[c]

[a]*Space Science and Engineering Division, Southwest Research Institute, 6220 Culebra Road, San Antonio, TX 78228, USA*
[b]*Lunar and Planetary Laboratory, University of Arizona, 1541 E University Boulevard, Tucson, AZ 85721, USA*
[c]*Space Sciences Laboratory, University of California Berkeley, 7 Gauss Way, Berkeley, CA 94720, USA*

Received 14 June 2006; received in revised form 23 August 2006; accepted 28 August 2006
Available online 20 December 2006

Abstract

We report global plasmasphere imaging observations from 20 March 2001 that show four main undulatory ripples propagating along the duskside plasmapause at an average westward azimuthal speed of 5 km/s. The aurora during this event showed some degree of temporal and spatial (both MLT and *L*-shell) correlation with the undulations, but this correlation was not nearly as strong as for a previous undulation event on 17 April 2001. Auroral intensifications preceded or coincided with the inception of all plasmapause indentations and undulations. However, there were several auroral enhancements at various latitudes that do not appear to have strong UT or MLT correlation with plasmapause motions. Auroral signatures that mapped closest to the *L* and MLT of the plasmapause were associated with the strongest, most long-lived plasmapause undulations, implying that magnetotail disturbances at lower *L* were more effective at distorting the plasmapause. Solar-wind-driven convection was strong, but relatively steady during the plasmapause undulations, and does not appear to have been directly responsible for them. This strong convection was apparently modulated by disturbances in the magnetotail that produced both the auroral signatures and the transient plasmapause distortions.

Keywords: Plasmasphere; Aurora; Inner magnetosphere; Substorm; Undulation

1. Background

1.1. The plasmasphere and plasmapause

The plasmasphere is the cold, dense torus of plasma that occupies the innermost portion of the magnetosphere. It is populated by outflow of ionospheric plasma, which fills plasmaspheric flux tubes with a mixture of H^+ (nominally 80–90%), He^+ (10–20%), and O^+ (a few percent) (Lemaire and Gringauz, 1998). Following extended periods of quiet geomagnetic conditions, the equatorial extent of the plasmasphere can be several Earth radii (R_E), with an internal density distribution that contains a great deal of fine-scale (under 0.1 R_E) and meso-scale (0.1–1 R_E) density structure (LeDocq et al., 1994; Carpenter, 1995; Sandel et al., 2001). Enhanced geomagnetic activity causes erosion of the plasmasphere, in which the outer plasma-filled flux tubes are caught up in the (low-latitude) convection

*Corresponding author. Tel.: +1 210 5225633; fax: +1 210 5209935.
E-mail address: jgoldstein@swri.edu (J. Goldstein).

1364-6826/$ - see front matter
doi:10.1016/j.jastp.2006.08.010

field and carried sunward, forming plumes of dense plasmaspheric material on the dayside (Grebowsky, 1970; Sandel et al., 2001; Goldstein et al., 2003a; Spasojević et al., 2003). The outer boundary of the plasmasphere, known as the plasmapause, arises from a dynamically changing imbalance between ionospheric filling and erosion. The extent and distribution of cold dense plasma is fundamental to the proper calculation of wave–particle interactions that control energetic particle populations (Albert, 2004), and is linked to structured ionospheric storm-enhanced density that can exert a strong space weather effect on communication and navigation (Su et al., 2001; Foster et al., 2002).

1.2. Externally and internally driven convection

Recent studies employing global images of the plasmasphere (Sandel et al., 2001) have shown that the inward or outward migration of the plasmapause can be directly driven by the solar wind and interplanetary magnetic field (IMF) conditions. In particular, southward IMF (generally thought to initiate sunward plasma convection in the inner magnetosphere) is strongly correlated with contraction or erosion of the nightside plasmapause and the creation of dayside plasmaspheric drainage plumes (Goldstein et al., 2003a; Spasojević et al., 2003). During northward IMF (thought to curtail sunward convection), the plasmapause can move outward quickly as a result of overshielding (Goldstein et al., 2002), or gradually as ionospheric outflow slowly refills formerly depleted flux tubes (Reinisch et al., 2004). Though global plasmapause dynamics are apparently dominated by the presence or absence of solar-wind-driven convection (Goldstein and Sandel, 2005), several key internal magnetospheric sources can contribute, including coupling to thermospheric winds (Sandel et al., 2003; Burch et al., 2004), shielding (Kelley et al., 1979; Goldstein et al., 2002), and subauroral polarization streams, or 'SAPS' (Foster et al., 2002; Foster and Burke, 2002; Goldstein et al., 2005a).

1.3. Substorm influence on the plasmapause

Decades of ground-based studies provide evidence that dipolarization of the tail magnetic field during substorms modulates the plasmapause location (Carpenter and Akasofu, 1972; Carpenter, 1995). Global plasmasphere images obtained on 17 April 2002 contain the first identified example of a striking undulatory motion of the duskside plasmapause, apparently triggered by a substorm dipolarization (Goldstein et al., 2004a, 2005b). The plasmapause undulation of 17 April 2002 consisted of a 0.4–1 R_E ripple that originated in the pre-midnight magnetic local time (MLT) sector, and subsequently propagated westward along the duskside plasmapause. Auroral images from this event contain evidence of a pre-midnight MLT substorm onset followed by a westward-traveling surge of auroral precipitation. Goldstein et al. (2005b) showed a close correspondence between the magnetically mapped auroral signature and the MLT-versus-UT trajectory of the plasmapause ripple, and concluded the undulation was triggered by the substorm. Analysis of the plasmapause motion and comparison with ring current images suggested the following chain of events: (1) the substorm dipolarization injected ring current plasma into the pre-midnight sector; (2) the pressure of the injected partial ring current inflated the magnetic field, pulling plasmaspheric plasma outward to form an initial bulge; (3) closure of the partial ring current through the ionosphere caused the formation of a SAPS flow channel that pushed the initial bulge westward, removing it and restoring the approximate original plasmapause location. At a fixed MLT, the signature of the undulation was a two-part plasmapause motion: the plasmapause first bulged outward, then moved inward to its approximate original L value. The 17 April undulation was thus a transient phenomenon, a traveling ripple that only temporarily distorted the plasmapause during its westward passage.

In this paper (as in Goldstein et al., 2005b), the term 'undulation' is meant to be descriptive of the motion of the plasmapause observed in global plasmasphere images. As discussed in the chain of events (1)–(3), plasmapause undulation appears to be caused by ring current injections and subsequent coupling between the partial ring current and the ionosphere. Thus, the plasmapause undulation is not a stand-alone motion, but is clearly part of a global response of the inner magnetosphere to the electrodynamic forcing provided by substorms. Although the undulatory motion has been associated with auroral activity (Goldstein et al., 2005b), it is important to distinguish plasmapause undulations from 'auroral undulations' that are apparently caused by drift waves at the inner edge of the plasma sheet (Lui et al., 1982; Lewis et al., 2005).

Despite the similar terminology, these are distinct phenomena arising from different causes.

Although traveling plasmapause ripples have been found to be associated with erosions in numerous events (Goldstein, 2006, and references therein), the 17 April 2002 event was the first reported example of the direct global plasmaspheric effect of substorm dipolarization. The close correspondence between the dynamic locations of the undulation and auroral precipitation found on 17 April suggests a very close coupling between the plasmasphere and the electron plasma sheet.

Both theoretical and observational studies predict that the evening sector inner edge of the electron plasma sheet should coincide with the Alfvén boundary (Thomsen et al., 2002; Korth et al., 1999), otherwise variously known as the last closed equipotential (LCE) or corotation-convection boundary (CCB). However, it is not generally the case that the evening sector LCE (or CCB) coincides with the plasmapause (Carpenter and Lemaire, 1997; Lemaire and Gringauz, 1998). This is so because the location and shape of the LCE change on the time scale of changes in the solar wind, whereas the plasmapause location changes either on the time scale of erosion (which takes a few to many hours, depending upon the strength of convection, and upon the MLT at which one observes the plasmapause) or on the time scale of refilling (which can take hours to days). The situation is further complicated by the fact that SAPS (mentioned above) can move the plasmapause well inside the duskside inner edge of the electron plasma sheet (Foster et al., 2002; Goldstein et al., 2003b). Thus, though both the electron plasma sheet and the plasmasphere are subject to the influence of convection, a one-to-one dynamic correspondence between the aurora and the plasmapause was a surprising result of the study of the 17 April 2002 substorm-initiated plasmapause undulation.

The generality of the global plasmapause–aurora correspondence during substorms is the topic of this paper. We present imaging observations of 20 March 2001, a day on which the duskside plasmapause experienced several westward-propagating undulations, each to some degree associated with an intensification and westward motion of an auroral precipitation signature. We will show, however, that the degree of spatial and temporal correlation between the undulations and the auroral signatures is not as strong as for the 17 April 2002 event previously studied by Goldstein et al. (2005b).

The rest of this paper is organized as follows. Section 2 describes how imaging data were analyzed to produce the plots. Section 3 interprets these plots and describes the 20 March multiple-undulation event. Section 4 summarizes the paper's results and lists some open questions.

2. Data analysis and description of plots

2.1. EUV plasmapause extraction

The global time-dependent plasmapause on 20 March 2001 was determined from images obtained by the extreme ultraviolet (EUV) imager onboard the Imager for Magnetopause-to-Aurora Global Exploration (IMAGE) satellite (Sandel et al., 2001). EUV plasmasphere images were created from 30.4-nm light resonantly scattered by He^+ ions, with a nominal cadence of 10 min and spatial resolution of 0.1 R_E or better. Plasmapause L and MLT points were manually extracted (Goldstein et al., 2003c) from 49 EUV images spanning the period 0933–1744 UT on 20 March. Eight global plasmapause shapes are plotted in Fig. 1. Each panel shows a single snapshot of the plasmapause L-versus-MLT shape. The plasmapause curves of Fig. 1 comprise (roughly) between 500 and 700 points each; this large number of points is sufficient to capture boundary features as small as one pixel ($<0.1\,R_E$), i.e., better than the usual (nominal) spatial uncertainty of 0.1–0.2 R_E (Goldstein et al., 2005c) of plasmapause extractions. Gaps in EUV plasmapause data near midnight, dawn, and noon are caused, respectively, by the Earth's shadow, imperfect flat-fielding between two adjacent cameras, and sunlight contamination.

2.2. EUV electric fields

Following Goldstein et al. (2005b), successive time snapshots of EUV plasmapause data were analyzed to infer an electric (E) field associated with the boundary motion. This technique yields the E-field component tangent to the moving boundary, $E_\pi \equiv V_P\,B\cos\alpha$, where $V_P = [\partial R_P/\partial t]_\varphi$ is the radial speed of the plasmapause at a fixed MLT (i.e., azimuthal angle φ), and B is the magnetic field strength. The angular term is defined as $\cos\alpha \equiv [1 + (1/R_P)^2(\partial R_P/\partial\varphi)_t^2]^{-1/2}$, where α is the angle between the azimuthal direction $\hat{\varphi}$ and the tangent to the plasmapause $\hat{\pi}$. If the plasmapause is circular, $\hat{\varphi} = \hat{\pi}$ and thus E_π is equal to azimuthal

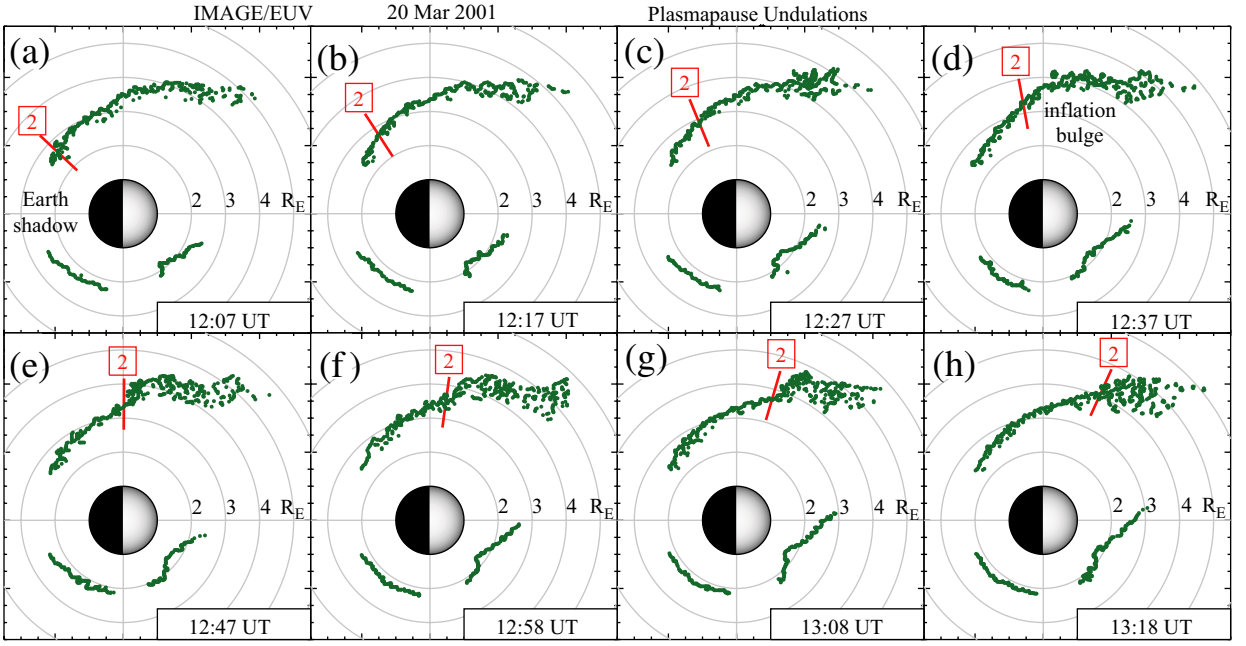

Fig. 1. Plasmapause locations obtained by IMAGE EUV, 20 March 2001. Each panel (a – h) shows a single snapshot of the global plasmapause shape, viewed in the SM-coordinate magnetic equatorial plane. The time of each snapshot is given in the lower right corner of the panel. The Sun is to the right; Earth in the center, with circles drawn at integer multiples of one Earth radius (R_E). The green dots are points manually extracted from EUV images (Goldstein et al., 2003c, 2005c); each panel contains approximately 500–700 plasmapause points. The line segments labeled '2' (corresponding to feature '2' in Fig. 2a) show the time-changing location of an undulatory ripple traveling along the duskside plasmapause.

electric field (E_φ). For a general plasmapause shape, E_π can represent both radial and azimuthal $E \times B$ drifts. For more details of the technique, see Goldstein et al. (2004b, 2005b) and Goldstein and Sandel (2005). In Fig. 2a, EUV E_π is presented in keogram format, with E-field (colored pixels) plotted versus MLT (vertical axis) and UT (horizontal axis). Negative E_π (yellow or red color) indicates inward and/or westward motion of the plasmapause. Positive E_π (blue) corresponds to outward/eastward motion. White pixels represent E_π magnitude less than 0.5 mV/m, and the gray area indicates the Earth's shadow, where no EUV plasmapause data were obtainable. Additional details of the E_π calculation for this paper can also be found in Section 3.1 (see discussion of small initial indentations).

2.3. FUV auroral data

Global images of auroral electron precipitation were obtained by the IMAGE far ultraviolet (FUV) imager SI-13 camera (Mende et al., 2000; Frey et al., 2003). The cadence of FUV images is 2 min; 256 FUV images spanning 0859–1740 UT were analyzed for this event. The result of this analysis is shown in Figs. 2b and c as MLT-versus-UT keogram plots in an arbitrary (normalized) intensity/color scale (red is most intense). FUV keograms are presented with two different ranges of magnetic latitude (Λ): Fig. 2b shows the entire auroral oval ($50-90^\circ\Lambda$) (the rationale for this latitude range is explained in Section 3.2), and Fig. 2c shows FUV intensity near the latitude of the EUV-observed plasmapause, for direct comparison with the EUV E-field keogram of Fig. 2a. To calculate each pixel of these keograms, averaging over latitude was performed, as follows. In Fig. 2b, each vertical slice represents one FUV image, and each pixel along that vertical slice is the auroral intensity at a single MLT, averaged over $50-90^\circ\Lambda$. In Fig. 2c, each pixel along a given vertical slice, i.e., at a single MLT, is the average FUV SI-13 intensity within $\pm3^\circ\Lambda$ of the plasmapause as determined for that MLT from the EUV image closest in time to the SI-13 image. Dipole mapping was employed to

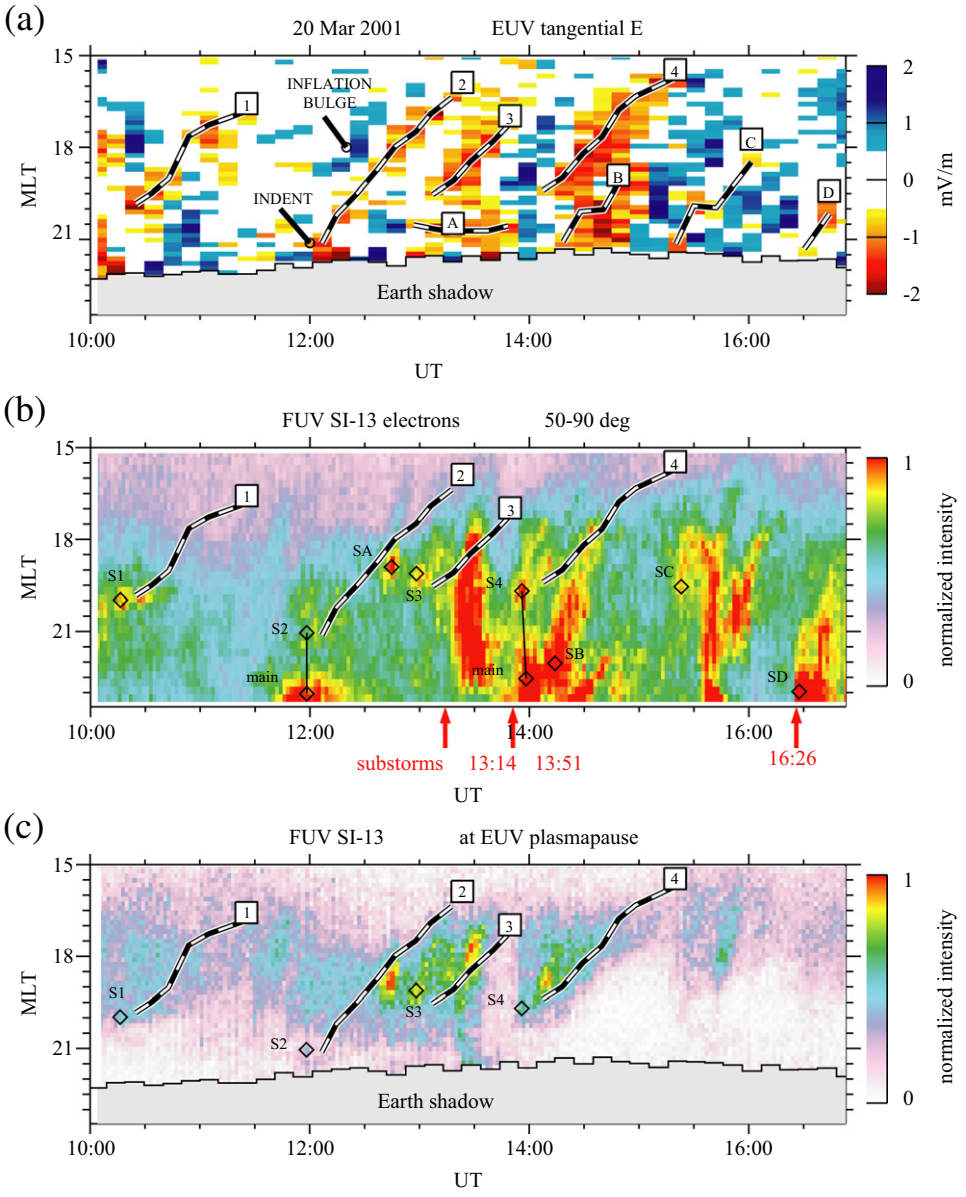

Fig. 2. Summary of 20 March 2001 observations from IMAGE EUV and FUV. (a) IMAGE EUV electric field E_π tangent to the plasmapause, deduced from plasmapause motion (Goldstein et al., 2004b), and plotted in MLT-versus-UT keogram format. Negative E_π (yellow, red) means inward and/or westward motion of the plasmapause; positive E_π (blue) means outward/eastward motion, as indicated by the colorbar (E_π magnitude smaller than 0.5 mV/m is white). Several key features are traced out with thick dashed lines: four main undulatory ripples (1, 2, 3, and 4) and several minor ripples (A–D). (b) IMAGE FUV SI-13 auroral keogram averaged over 50–90°magnetic latitude (Λ), in normalized intensity scale (red = most intense). Three substorm onsets are indicated by arrows at the bottom of the plot. For comparison, plasmapause ripples 1–4 (from Fig. 2a) are indicated by dashed lines and labels. Several SI-13 ('S') auroral features corresponding to plasmapause ripples are also labeled S1–S4 and SA–SD. Note S2 and S4 are MLT-local features linked to global brightenings ('main'). (c) IMAGE FUV auroral data, format similar to Fig. 2b, but here each pixel is the average FUV intensity within $\pm 3^\circ\Lambda$ of the EUV plasmapause location. The undulations are correlated with auroral activity at plasmapause latitudes.

calculate the plasmapause latitude Λ. The dipole assumption is reasonable for the small size ($L \approx 2-4$) of the observed plasmapause, and the $\pm 3^\circ$ averaging minimizes the impact (on our results) of deviation of the real magnetic field from this simple assumption.

3. Plasmapause undulations of 20 March 2001

3.1. Plasmapause observations, 20 March 2001

Between 1000 and 1700 UT on 20 March 2001, several traveling ripples passed along the duskside plasmapause, producing an undulatory motion. When viewed in an animated sequence of EUV data, this motion evokes the mental image of shaking dust out of a rug, or waves on the surface of the ocean.[1] The motion was quite complex, involving multiple undulations that at times comprised very subtle (0.1–0.2 R_E) distortions of the plasmapause shape. The intrinsically dynamic nature of the undulations was quantitatively captured by analyzing the speed (V_P) of the plasmapause to infer the electric field E_π (see Section 2.2). As described below, we used E_π data to identify four main undulation signatures ('1' through '4'). In the discussion immediately following, the EUV data for this event are presented in two ways, as a series of eight individual plasmapause snapshots highlighting a single undulation (Fig. 1), and as an electric field (E_π) keogram of the entire event (Fig. 2a).

The start-to-finish evolution of undulation 2 is depicted in the series of eight plasmapause snapshots of Figs. 1a–h. In each individual frame, the plasmapause indentation associated with undulation 2 is indicated by a radial line segment labeled '2'. (As described below, the MLT of the line segment at a given UT was obtained directly from analysis of E_π data.) As shown by Figs. 1a–h, undulation 2 propagated westward from 2107 to 1623 MLT during the interval 1207–1318 UT. Undulation 2 began as a 0.1–0.2 R_E plasmapause indentation at (1207 UT, 2107 MLT) that grew in size as it propagated westward. (This initial indentation is labeled 'INDENT' in Fig. 2a.) After 1237 UT the indentation was roughly 1 R_E in radial size, as most clearly exemplified by the step-like increase of plasmapause L-value (from $L \approx 3$ to 4) at 1800 MLT in the 1247 UT snapshot (Fig. 1e). Perhaps related to this later undulation growth, the arrival of the indentation at (1247 UT, 1759 MLT) was preceded at 1227 UT by the formation of a bulge near 1800 MLT (labeled in Figs. 1d and 2a). That is, at 1800 MLT undulation 2 consisted of two components: first a bulge formed, and then an undulation passed by and removed the bulge, restoring the plasmapause to its (approximate) original L-value at that MLT. The formation of this plasmapause bulge (just before its removal by a traveling ripple) is similar to that observed for the 17 April 2002 undulation, which Goldstein et al. (2004a) explained as arising from magnetic inflation by substorm-injected ring current pressure. Consistent with this explanation, between 1200 and 1300 UT the Sym-H geomagnetic index (available online; see Acknowledgements) contained a −20 nT reduction (from −147 to −167 nT), half of which occurred before 1240 UT. The possible role of this inflation-produced bulge in the late-stage undulation growth will be revisited in Section 3.2 discussion of the auroral observations.

In the 20 March event, the dominant signature associated with the passage of an undulation seemed to be a local plasmapause inward motion or indentation ($V_P < 0$). As was true for undulation 2, in some of the other undulations the plasmapause reduction was preceded or followed by an outward motion or bulge ($V_P > 0$), such that there was no net effect on R_P of the undulation's passage. Thus, in the E_π keogram of Fig. 2a the westward-moving undulations appear as a series of intense yellow or red diagonal stripes ($E_\pi < -0.5$ mV/m), interspersed with some generally less intense blue diagonal stripes ($E_\pi > +0.5$ mV/m). The four main undulations for this event are labeled '1' through '4', and their MLT-versus-UT trajectories are traced with thick black and white dashed lines. Several minor features are similarly traced, and labeled 'A' through 'D'. Because the undulations at times involved very small plasmapause displacements (as further discussed below), it was the E_π keogram that was used to identify the undulations and extract their (MLT, UT) trajectories. Visual classification of 1–4 as the main undulatory features in the E_π keogram used the following criteria: $E_\pi < -1$ mV/m somewhere along the diagonal, overall duration at least 40 min, and continuity (or coherence) of the red/yellow diagonal features (this last criterion is the most subjective). These criteria adequately reflect that 1–4 are the undulatory motions that appear most conspicuously in the animated sequence of EUV images.

It was mentioned earlier that undulation 2 began as a small (0.1–0.2 R_E) indentation that later grew in size. Such small initial indentations are difficult to identify in individual snapshots (Figs. 1a–c), though they are readily discernible in animations of EUV

[1]This animated EUV image sequence is available at the URL http://enarc.space.swri.edu/PAPERS/FTP/DusksideUndulations/ppa_movie.GIF

data, and in the E_π keogram (Fig. 2a). The quantity E_π is determined from the plasmapause speed V_P, which according to the technique of Goldstein et al. (2004b) is calculated as a centered-difference time derivative of plasmapause location R_P. Fig. 3 illustrates how small indentations are identified through such a calculation. Each plot shows a close-up view of the duskside plasmapause L-versus-MLT during the passage of undulation 2. For each UT, two curves of EUV plasmapause data are plotted, from ± 10 min relative to the UT of the plot. The earlier-in-time data are given by circles and the thinner (blue) curve; the later EUV data are the '+' symbols and the thicker (red) curve. The solid curves are Fourier expansions of the EUV data points, which allow calculation of V_P as a single-valued function of MLT (Goldstein et al., 2004b). In each case, the later EUV plasmapause is at least 0.1 R_E inward of the earlier location; for reference, the thick vertical bar indicates 0.1 R_E scale. When evaluating the accuracy of the measured displacements, the scatter in the data points may also be considered a measure of the uncertainty. Except in the 1227 UT snapshot (Fig. 3c), the spatial separation between the earlier and later EUV data curves in Fig. 3 clearly exceeds the scatter of the points of each curve.

How believable are plasmapause displacements 0.1 R_E in size? Despite nominal EUV plasmapause L uncertainty of 0.1–0.2 R_E (Goldstein et al., 2005c), two factors argue in favor of trusting these 0.1-R_E displacements. First, the plasmapause for the 20 March 2001 event was extracted with much greater precision than usual; features as small as one pixel (often <0.1 R_E in size, especially at the small L values of this event) were painstakingly traced out for this event. Second, the small plasmapause displacements observed at the inception of each undulation were part of a larger global pattern evident in the E_π keograms. For example, though the initial indentation of undulation 2 was small, its E_π signature during 1207–1237 UT is clearly part of the larger diagonal MLT-versus-UT line labeled '2' in Fig. 2a, with E-field magnitude (about 1–2 mV/m) that is consistent with the rest of the diagonal signature.

Another presentation of the IMAGE EUV data is given in Fig. 4, produced as follows. From each UT snapshot of EUV data, a 100-term Fourier expansion of plasmapause L-versus-MLT was computed at 26 regularly spaced (0.15-h spacing) MLT values spanning 1600–1954 MLT. At each of these 26 MLT values, an L-versus-UT curve was produced from the Fourier expansions. For each of the 26 L-versus-UT curves, a plasmapause residual ΔL was calculated by subtracting the mean L from the interval 1000–1700 UT. Each of the plasmapause residuals ΔL was added to its respective MLT value to produce Fig. 4, a plot of $(\mathrm{MLT}+\Delta L)$-versus-UT. Thus, plasmapause residuals appear as deflections (up or down) from the horizontal (i.e., constant MLT). In this plot (as in Fig. 2), the MLT-axis is reversed, so that indentations of the plasmapause (i.e., $\Delta L<0$) are given by upward deflections. Red portions of the 26 curves indicate where $\mathrm{d}L/\mathrm{d}t \leqslant -0.1/(10\ \mathrm{min})$, i.e., where the plasmapause moved inward more than 0.1 R_E in a single EUV timestep (10 min). Overplotted are the $(\mathrm{MLT}+\Delta L)$-versus-UT trajectories of the four major undulatory ripples (1–4) from Fig. 2, which agree with the red sections. We interpret this agreement as support for our independent identification (in Fig. 2) of the four main undulations.

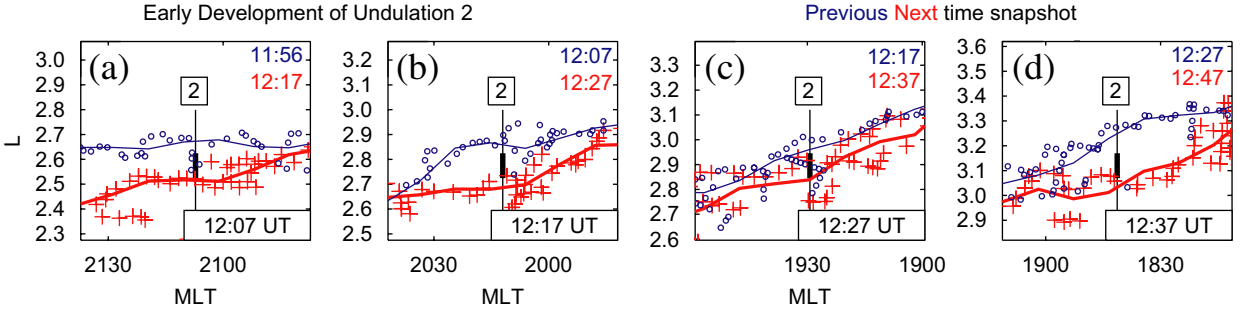

Fig. 3. Close-up view of the westward moving undulation 2 (1207–1237 UT). Shown are plasmapause L values versus MLT, spanning 1 MLT-hour and centered at the MLT-location of the ripple (vertical line '2'). Compare panels a–d with Figs. 1a–d. The solid curves are 100-term Fourier expansions of the EUV plasmapause data ('+' or circles). The thicker (thinner) curve shows data from the next (previous) snapshot, used for a centered-difference calculation of V_P. (See text.) UT times of previous (next) snapshots given at top right corner. The thick vertical bar centered at '2' indicates 0.1R_E scale size.

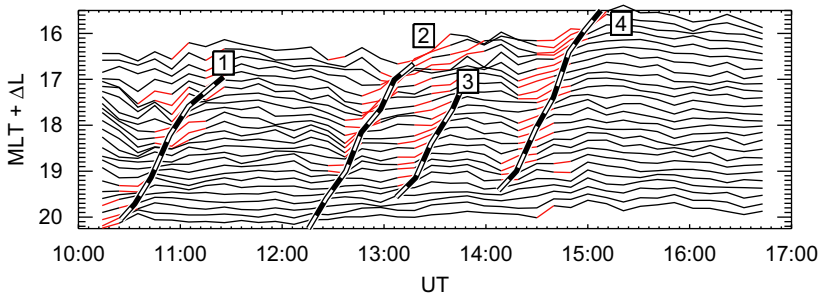

Fig. 4. Alternate depiction of the four major westward-moving plasmapause undulations of 20 March 2001. As described in text, shown are 26 plasmapause residual curves (MLT + ΔL)-versus-UT, derived from IMAGE plasmapause data (such as shown in Fig. 1). In each of the 26 curves, plasmapause indentations appear as upward deflections, and red portions of the curves indicate where $dL/dt < -0.1\,R_E/(10\text{ min})$.

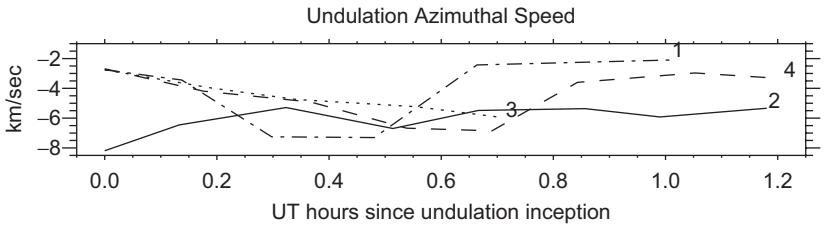

Fig. 5. Azimuthal speed (km/s) of the four major westward-moving plasmapause undulations, versus number of UT hours since inception of each undulation.

Fig. 4 illustrates that the passage of each of the undulatory ripples appears at a fixed MLT as an inward plasmapause displacement, in some cases preceded or followed by an outward displacement. For example, near 1800 MLT and preceding undulation 2, a pre-undulatory plasmapause inflation can be seen as a downward excursion. By examining the full range of MLT, the plasmapause displacements at individual MLT values are shown to be part of a global MLT-versus-UT pattern.

As shown by Goldstein et al. (2005b), the MLT-versus-UT trajectories of plasmapause undulations yield information about the azimuthal flow speed at the plasmapause. The azimuthal flows found for this event are comparable to those reported for the 17 April 2002 undulation. Undulations 2–4 all have an average (per undulation) slope of −3 MLT-h/UT-h; undulation 1 has a slightly higher slope of −4 MLT-h/UT-h. Fig. 5 shows azimuthal flow speeds for undulations 1–4, calculated using the per-EUV-image MLT, UT, and plasmapause L for each undulation. The negative speed denotes westward motion. Magnitudes range from a minimum of 2 km/s (undulation 1, 1 h after inception) to a peak of 8 km/s (undulation 2, at inception), with an overall average (for all undulations) of 5 km/s. Note that these are net azimuthal speeds; subtracting the eastward corotational flow (varying between 1.4 and 1.9 km/s depending on the plasmapause L) yields an overall average magnitude of 6.4 km/s for the flows in the corotating frame.

3.2. Auroral observations, 20 March 2001

Goldstein et al. (2004a, 2005b) hypothesized that undulatory plasmapause ripples might be caused by magnetic and convective disturbances associated with auroral intensifications (e.g., substorms), based in part on the spatial and temporal correspondence between the plasmapause and aurora on 17 April 2002. To test whether this correspondence applies to the 20 March 2001 event, Figs. 2b and c show auroral data for comparison with the E_π keogram. The black and white dashed lines in Figs. 2b and c trace out the MLT-versus-UT trajectories of the four major plasmapause undulations (1–4) of 20 March.

Fig. 2b shows a keogram of the entire auroral oval. The rationale for showing the entire oval is to facilitate identification of substorm onsets (by the reader) and provide a global context for auroral signatures that are more localized to the plasmapause. Substorm identifications were obtained from

IMAGE FUV images (which contain more information than the keogram of Fig. 2b) by the third author (Frey et al., 2004). During the period 1000–1700 UT IMAGE FUV witnessed three substorms (labeled with red arrows in Fig. 2b), and a number of auroral intensifications including a pseudo-breakup at 1530 UT. Several of these SI-13 ('S') auroral features can be associated with the inceptions of plasmapause features 1–4 and A–D in Fig. 2a. The (MLT, UT) coordinate of each such associated auroral feature is indicated by a small diamond, and each diamond is labeled 'S*N*' where *N* is a number or letter matching the label of one of the plasmapause features. For example, the auroral feature associated with the start of undulation 1 is labeled 'S1'. In the discussion of Fig. 2b two types of correlation will be discussed, 'UT' and 'MLT'. Here UT correlation means that the auroral feature either directly preceded or was coincident with the inception of a plasmapause feature. MLT correlation means that the auroral feature also appeared at the same MLT as the plasmapause feature inception.

The four main plasmapause undulations (1–4) all had auroral features that were to some degree correlated in both UT and MLT (S1–S4). As discussed below, however, the correlation is circumstantial and should certainly be subjected to further investigation. Undulations 1 and 3 were preceded by auroral intensifications (S1 and S3) that were limited to the MLT vicinity of the first appearance of the undulations. Undulations 2 and 4 also had MLT-local auroral intensifications (S2 and S4), but these auroral features were linked to (or part of) global auroral brightenings (labeled 'main'). For example, undulation 4 was preceded by S4, which was part of the 1351 UT substorm onset ('main', between 2130 and 2400 MLT). Auroral features (S1, S2, S3, S4) occurred within (0.1, 0.1, 0.4, 0.3) MLT-hours of the inceptions of their respective plasmapause undulations (1, 2, 3, 4).

The plasmapause indentations A–D also exhibit some degree of UT and MLT correlation with auroral intensifications SA–SD, though the correlation is in some cases more questionable than that of main undulations 1–4. The MLT agreement is generally worse: auroral features (SA, SB, SC, SD) occurred within (1.6, 1.0, 1.5, 1.5) MLT-hours of the inceptions of their respective plasmapause undulations (A, B, C, D). Though SA preceded the inception of indentation A, the strongest E_π for this signature occurred after the 1314 UT substorm. On the other hand, the general MLT extent and UT duration of SB, SC, and SD agree quite well with their respective indentations B, C, and D.

It was mentioned earlier (Section 3.1) that undulations 2 and 3 started as small plasmapause distortions that grew larger (or were amplified) with time. This late-stage amplification is evident as expansion of the size of the indentation/ripple (e.g., Fig. 1e), as well as increases in the magnitude of E_π in Fig. 2a. The late-stage amplification effect is temporally correlated with auroral signatures. Both undulation 3 and indentation A were amplified (E_π magnitude increased by 25–50%, and the MLT extent quadrupled) after the 1314 UT substorm. Auroral feature SA (1245 UT) coincided with an amplification of undulation 2 (noted earlier) in which its radial size increased from 0.1 to 1 R_E. Thus, based on this circumstantial evidence, it is possible that the auroral intensification could have been related to these late-stage amplifications.

However, a more likely explanation involves the duskside plasmapause inflation that preceded the arrival of undulation 2 at 1800 MLT (see earlier discussion of Fig. 1). We contend that inflation and bulge formation (produced by substorm ring current injections) can precondition the plasmapause to produce larger undulations, as follows. The undulation effect arises in part from an inward plasmapause displacement produced by SAPS (Goldstein et al., 2005b). The strength and radial extent of SAPS are determined by the configuration of the ring current, and to first approximation can be treated as independent of the plasmapause location. A stronger inward plasmapause displacement will result if, at the inception of the SAPS effect, the plasmapause bulges farther out into the SAPS flow channel. This is a generalization of the fact that a given convection enhancements will produce a more profound effect on a larger (i.e., more refilled) plasmasphere than on an already eroded plasmasphere. In the same way, a given SAPS flow channel will produce a stronger undulatory indentation if the plasmapause is located at larger *L*.

We have just described how auroral intensifications preceded or coincided with the inceptions of each of the plasmapause indentations and undulations. However, it must be noted that there were several auroral enhancements at various latitudes that do not appear to have strong UT or MLT correlation with plasmapause motions, and regardless, such correlation is circumstantial. For the correlation to be meaningful, electromagnetic

disturbances in the magnetotail must produce aurora and also must have an effect on the plasmapause. Auroral activity at lower latitudes (reflecting magnetotail disturbances at lower L) should therefore correlate more closely with plasmapause motion. To examine the latitudinal (or L-shell) correlation between aurora and plasmapause, Fig. 2c presents data extracted from FUV pixels within $\pm 3^{\circ}\Lambda$ of the EUV plasmapause. The intensity scale of this 'plasmapause-vicinity' keogram is the same as that of the full-oval keogram. From Fig. 2c it is clear that the four major undulations (1–4) all happened in conjunction with significant auroral activity close to the plasmapause. Comparison between Fig. 2a and c should convince the reader that the stronger the auroral signature near the plasmapause, the more intense, long-lived, and continuous the undulation. Furthermore, the general MLT-versus-UT trend of the near-plasmapause auroral activity follows the trajectories of the undulations. However, for this 20 March 2001 event the MLT-versus-UT correlation between the 'plasmapause-vicinity' aurora and the plasmapause motion is not nearly as good as that of the 17 April 2002 event.

How should plasmapause–aurora correspondence be interpreted? First, if the magnetic disturbances associated with the auroral activity are causing the plasmapause undulations, then the closer (in L) the auroral disturbance, the more pronounced the plasmapause distortion. Auroral events reaching lower latitudes are probably more likely to be associated with plasmapause undulations. Second, it is possible that the coincidence of the auroral activity and the plasmapause undulations reflects that the plasma sheet and plasmapause respond to disturbances (originating in the magnetotail) with some degree of spatial and temporal coherence. Said another way, the plasma sheet and plasmapause may respond together as a single coupled system. The details of this response demand further investigation, since in principle, westward expansion of the substorm precipitation should not be directly related to actual drifts of electrons in the plasma sheet (which would tend to drift eastward following the substorm injection).

3.3. Solar wind and IMF observations, 20 March 2001

The keogram plots of Fig. 2 strongly suggest a close correspondence (both spatial and temporal) between the aurora and plasmapause on 20 March. This section examines what aspects of plasmapause behavior on 20 March were directly driven by conditions in the solar wind and IMF. In Fig. 6 are shown data from the Advanced Composition Explorer (ACE) spacecraft (Stone et al., 1998), delayed 1 h to account for solar wind propagation to the magnetopause from ACE's upstream location. The vertical lines give the starting times of each of the plasmapause features 1–4 and A–D from Fig. 2a. Although there was on 20 March a normal degree of fluctuation of solar wind and IMF quantities, during the first three major undulations (1–3) conditions were relatively steady. For example, during 1000–1400 UT, the B_z component varied only 1.5 nT (8%) from its average value of -18 nT. Looking at Fig. 6, there is nothing systematic in the fluctuations of the ACE data that can explain all of

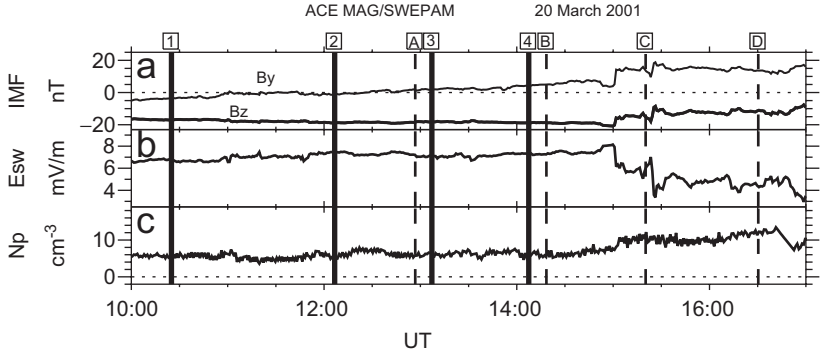

Fig. 6. Interplanetary magnetic field (IMF) and solar wind data from ACE MAG (Smith et al., 1998) and SWEPAM (McComas et al., 1998) instruments. The vertical lines are the start times of each of the undulatory ripple features (1–4 and A–D) from Fig. 2a. (a) IMF B_z and B_y. (b) Solar wind E-field $E_{SW} = V_{SW} B_z$. (c) Solar wind proton density. Solar-wind-driven convection, though strong, does not appear to have been directly responsible for the plasmapause undulations. (See text.)

the plasmapause dynamics. For example, fluctuations in B_y might (in principle) cause some dawn–dusk 'flapping' of the drainage plume, but there is not a B_y fluctuation signature common to all the undulations.

We hypothesize that the solar wind and IMF did not directly drive the plasmapause undulations, but did provide preconditioning in the form of strong convection. The steady, strongly negative B_z (and 6–8 mV/m solar wind E-field) presumably exerted a direct control on the plasmasphere by driving steady and strong sunward convection. This presumption is well supported by the eroded state of the plasmasphere during this event (see Fig. 1); the reduced ($L \approx 2$) dawnside plasmapause and sunward-pointing dayside drainage plume are well-documented byproducts of strong sunward convection during southward B_z (Goldstein and Sandel, 2005). This strong sunward convection created the duskside plume and exerted zero-order (dominant) control of the dusk location of the plasmapause. Based on the agreement with auroral data, it seems most likely that the actual undulations were directly triggered by activity in the magnetotail (i.e., internal to the magnetosphere).

4. Conclusions

We have reported global plasmasphere imaging observations from 20 March 2001, showing multiple undulatory ripples propagating along the duskside plasmapause at an average westward azimuthal speed of 5 km/s in the fixed frame, 6 km/s in the corotating frame. Auroral data contained signatures with some degree of temporal and spatial (both MLT and L-shell) correlation with the dynamic plasmapause location. Auroral intensifications preceded or coincided with the inception of all plasmapause indentations and undulations. However, there were several auroral enhancements at various latitudes that do not appear to have strong UT or MLT correlation with plasmapause motions. Auroral signatures that mapped closest to the L and MLT of the plasmapause were associated with undulations (1–4) that were the most intense, long-lived, and continuous. This implies that magnetotail disturbances at lower L were more effective at distorting the plasmapause.

Solar-wind-driven convection was strong, but relatively steady during the plasmapause undulations, and does not appear to have been directly responsible for them. This strong convection was apparently modulated by disturbances in the magnetotail that produced both the auroral signatures and a transient convection that only temporarily distorts the plasmapause. After the passage of each of the undulations, the duskside plasmapause returned approximately to its pre-undulation location. This study demonstrates that the plasmapause undulation effect observed (in a previous study) on 17 April 2002 (Goldstein et al., 2004a, 2005b) was not a unique occurrence. It seems likely that transient plasmapause undulations and indentations routinely result from magnetotail disturbances that cause substorms and auroral intensifications.

The correspondence between the behavior of the plasmapause and aurora requires the ability to examine these two phenomena from a global, systems-level perspective. This correspondence suggests that the plasmasphere and plasma sheet respond to substorms and magnetotail disturbances as a single coupled system. Questions still remain about the driver and details of that response. Do plasmapause undulations reflect a global, propagating impulse front that sweeps through the inner magnetosphere, or are they surface waves akin to the flapping of a flag in a strong breeze? Are the plasma sheet and plasmasphere truly both responding to the same disturbance, or do the auroral intensifications result from the disturbance and then in turn directly produce the undulation? Knowing that electrons drift eastward, what causes the auroral signature to propagate westward alongside the plasmapause ripple? In future work, further systems-level analysis should be applied to the study of such events.

Acknowledgments

We thank N. Ness, C. Smith, D. McComas, and the excellent ACE science center for providing easy access to solar wind data and IMF data, and the World Data Center for Geomagnetism, Kyoto, for online access to Sym-H data. Discussions with W. Lewis, J. Burch, and various members of the IMAGE science team are gratefully acknowledged. Financial support was generously provided by NASA Grants NAG5-12787 and NAS5-96020.

References

Albert, J.M., 2004. Using quasi-linear diffusion to model acceleration and loss from wave-particle interactions. Space Weather 2, S09S03.

Burch, J.L., Goldstein, J., Sandel, B.R., 2004. Cause of plasmasphere corotation lag. Geophysical Research Letters 31, L05802.

Carpenter, D.L., 1995. Earth's plasmasphere awaits rediscovery. EOS Transactions AGU 76, 89.

Carpenter, D.L., Akasofu, S.-I., 1972. Two substorm studies of relations between westward electric fields in the outer plasmasphere, auroral activity, and geomagnetic perturbations. Journal of Geophysical Research 77, 6854.

Carpenter, D.L., Lemaire, J., 1997. Erosion and recovery of the plasmasphere in the plasmapause region. Space Science Reviews 80, 153.

Foster, J.C., Burke, W.J., 2002. SAPS: a new categorization for sub-auroral electric fields. EOS Transactions AGU 83, 393.

Foster, J.C., Erickson, P.J., Coster, A.J., Goldstein, J., 2002. Ionospheric signatures of plasmaspheric tails. Geophysical Research Letters 29 (13), 1623.

Frey, H.U., Mende, S.B., Angelopoulos, V., Donovan, E.F., 2004. Substorm onset observations by IMAGE-FUV. Journal of Geophysical Research 109, A10304.

Frey, H.U., et al., 2003. Summary of quantitative interpretation of IMAGE far ultraviolet auroral data. Space Science Reviews 109, 255.

Goldstein, J., 2006. Plasmasphere response: tutorial and review of recent imaging results. Space Science Reviews 124, in press.

Goldstein, J., Sandel, B.R., 2005. The global pattern of evolution of plasmaspheric drainage plumes. In: Burch, J.L., Schulz, M., Spence, H. (Eds.), Inner Magnetosphere Interactions: New Perspectives from Imaging. American Geophysical Union, Washington, DC, p. 1.

Goldstein, J., Spiro, R.W., Reiff, P.H., Wolf, R.A., Sandel, B.R., Freeman, J.W., Lambour, R.L., 2002. IMF-driven overshielding electric field and the origin of the plasmaspheric shoulder of May 24, 2000. Geophysical Research Letters 29 (16).

Goldstein, J., Sandel, B.R., Forrester, W.T., Reiff, P.H., 2003a. IMF-driven plasmasphere erosion of 10 July 2000. Geophysical Research Letters 30 (3).

Goldstein, J., Sandel, B.R., Reiff, P.H., Hairston, M.R., 2003b. Control of plasmaspheric dynamics by both convection and sub-auroral polarization stream. Geophysical Research Letters 30 (24), 2243.

Goldstein, J., Spasojević, M., Reiff, P.H., Sandel, B.R., Forrester, W.T., Gallagher, D.L., Reinisch, B.W., 2003c. Identifying the plasmapause in IMAGE EUV data using IMAGE RPI in situ steep density gradients. Journal of Geophysical Research 108 (A4), 1147.

Goldstein, J., Sandel, B.R., Hairston, M.R., Mende, S.B., 2004a. Plasmapause undulation of 17 April 2002. Geophysical Research Letters 31, L15801.

Goldstein, J., Wolf, R.A., Sandel, B.R., Reiff, P.H., 2004b. Electric fields deduced from plasmapause motion in IMAGE EUV images. Geophysical Research Letters 31 (1), L01801.

Goldstein, J., Burch, J.L., Sandel, B.R., 2005a. Magnetospheric model of subauroral polarization stream. Journal of Geophysical Research 110, A09222.

Goldstein, J., Burch, J.L., Sandel, B.R., Mende, S.B., Cson Brandt, P., Hairston, M.R., 2005b. Coupled response of the inner magnetosphere and ionosphere on 17 April 2002. Journal of Geophysical Research 110, A03205.

Goldstein, J., Sandel, B.R., Forrester, T.F., Thomsen, M.F., Hairston, M.R., 2005c. Global plasmasphere evolution 22–23 April 2001. Journal of Geophysical Research 110, A12218.

Grebowsky, J.M., 1970. Model study of plasmapause motion. Journal of Geophysical Research 75, 4329.

Kelley, M.C., Fejer, B.G., Gonzales, C.A., 1979. An explanation for anomalous ionospheric electric fields associated with a northward turning of the interplanetary magnetic field. Geophysical Research Letters 6, 301.

Korth, H., Thomsen, M.F., Borovsky, J.E., McComas, D.J., 1999. Plasma sheet access to geosynchronous orbit. Journal of Geophysical Research 104, 25407.

LeDocq, M.J., Gurnett, D.A., Anderson, R.R., 1994. Electron number density fluctuations near the plasmapause observed by the CRRES spacecraft. Journal of Geophysical Research 99, 23661.

Lemaire, J.F., Gringauz, K.I., 1998. The Earth's Plasmasphere. Cambridge University Press, Cambridge.

Lewis, W.S., Burch, J.L., Goldstein, J., Horton, W., Perez, J.C., Frey, H.U., Anderson, P.C., 2005. Duskside auroral undulations observed by IMAGE and their possible association with large-scale structures on the inner edge of the electron plasma sheet. Geophysical Research Letters 32, L24103.

Lui, A.T.Y., Meng, C.-I., Ismail, S., 1982. Large-amplitude undulations of the equatorward boundary of the diffuse aurora. Journal of Geophysical Research 87, 2385.

McComas, D.J., Bame, S.J., Barker, P., Feldman, W.C., Phillips, J.L., Riley, P., Griffee, J.W., 1998. Solar wind electron proton alpha monitor (SWEPAM) for the advanced composition explorer. Space Science Reviews 86, 563.

Mende, S.B., Heetderks, H., Frey, H.U., Stock, J.M., Lampton, M., Geller, S.P., Abiad, R., Siegmund, O.H.W., Habraken, S., Renotte, E., Jamar, C., Rochus, P., Gerard, J.-C., Sigler, R., Lauche, H., 2000. Far ultraviolet imaging from the IMAGE spacecraft. 3. Spectral imaging of Lyman-α and OI 135. 6 nm. Space Science Reviews 91, 287.

Reinisch, B.W., Huang, X., Song, P., Green, J.L., Fung, S.F., Vasyliunas, V.M., Gallagher, D.L., Sandel, B.R., 2004. Plasmaspheric mass loss and refilling as a result of a magnetic storm. Journal of Geophysical Research 109, A01202.

Sandel, B.R., King, R.A., Forrester, W.T., Gallagher, D.L., Broadfoot, A.L., Curtis, C.C., 2001. Initial results from the IMAGE extreme ultraviolet imager. Geophysical Research Letters 28, 1439.

Sandel, B.R., Goldstein, J., Gallagher, D.L., Spasojević, M., 2003. Extreme ultraviolet imager observations of the structure and dynamics of the plasmasphere. Space Science Reviews 109, 25.

Smith, C.W., Acuna, M.H., Burlaga, L.F., L'Heureux, J., Ness, N.F., Sheifele, J., 1998. The ACE magnetic field experiment. Space Science Reviews 86, 613.

Spasojević, M., Goldstein, J., Carpenter, D.L., Inan, U.S., Sandel, B.R., Moldwin, M.B., Reinisch, B.W., 2003. Global response of the plasmasphere to a geomagnetic disturbance. Journal of Geophysical Research 108 (A9), 1340.

Stone, E.C., Frandsen, A.M., Mewaldt, R.A., Christian, E.R., Margolies, D., Ormes, J.F., Snow, F., 1998. The advanced composition explorer. Space Science Reviews 86, 1.

Su, Y.-J., Thomsen, M.F., Borovsky, J.E., Foster, J.C., 2001. A linkage between polar patches and plasmaspheric drainage plumes. Geophysical Research Letters 28, 111.

Thomsen, M.F., Korth, H., Elphic, R.C., 2002. Upper cutoff energy of the electron plasma sheet as a measure of magnetospheric convection strength. Journal of Geophysical Research 107 (A10), 1331.